

Kron reduction methods for plug-and-play control of ac islanded microgrids with arbitrary topology

Michele Tucci^{*1}, Alessandro Floriduz^{† 1}, Stefano Riverso^{‡2}, and Giancarlo Ferrari-Trecate^{§ 1}

¹*Dipartimento di Ingegneria Industriale e dell'Informazione, Università degli Studi di Pavia*

²*United Technologies Research Center Ireland*

Technical Report
October, 2015

Abstract

In this paper, we provide an extension of the scalable algorithm proposed in [1] for the design of Plug-and-Play (PnP) controllers for AC Islanded microGrids (ImGs). The method in [1] assumes Distributed Generation Units (DGUs) are arranged in a load-connected topology, i.e. loads can appear only at the output terminals of inverters. For handling totally general interconnections of DGUs and loads, we describe an approach based on Kron Reduction (KR), a network reduction method giving an equivalent load-connected model of the original ImG. However, existing KR approaches can fail in preserving the structure of transfer functions representing transmission lines. To avoid this drawback, we introduce an approximate KR algorithm, still capable to represent exactly the asymptotic periodic behavior of electric signals even if they are unbalanced. Our results are backed up with simulations illustrating features of the new KR approach as well as its use for designing PnP controllers in a 21-bus ImG derived from an IEEE test feeder.

Keywords: Kron reduction, graph theory, islanded microgrid, plug-and-play, decentralized control, voltage and frequency control.

^{*}Electronic address: michele.tucci02@universitadipavia.it; Corresponding author

[†]Electronic address: alessandro.floriduz012@universitadipavia.it

[‡]Electronic address: RiversS@utrc.utc.com

[§]Electronic address: giancarlo.ferrari@unipv.it

1 Introduction

Kron Reduction (KR) is one of the most popular methods for simplifying linear electrical networks [2] while preserving the behavior of electrical variables at target nodes. Widely used with phasor voltages and currents, KR assumes network nodes are classified either as internal or boundary nodes and it provides an algebraic procedure for computing: (i) the topology of a new network connecting boundary nodes only, (ii) the value of admittances related to new edges and (iii) equivalent currents supplied at boundary nodes accounting for the effect of internal currents in the original network. Graph-theoretical properties of KR have been analyzed in [3] and [4] for DC resistive networks. A generalization to AC three-phase balanced circuits in Periodic Sinusoidal Steady State (PSSS), which will be termed AC-KR, can be found in [5]. Recently, several studies focused on generalizations of KR preserving the value of electric boundary variables not only in the asymptotic regime, but also during transients [3, 5, 6, 7, 8]. In these *instantaneous* KR procedures, line admittances are replaced by differential models and sufficient conditions guaranteeing well-posedness of the network reduction process have been studied.

KR finds applications also to Islanded microGrids (ImGs), i.e. autonomous energy islands disconnected from the main grid and composed of the interconnection of DGUs and loads [9]. For instance, in [7] and [10] KR is advocated as the key tool for mapping ImGs with a general topology into a standard topology (called *load-connected*) where loads appear only at the terminals of inverters. This can be done labeling the nodes of loads not directly connected to inverter terminals as internal nodes and applying KR to eliminate them. As a consequence, KR can also impact on the design of decentralized control schemes where local controllers associated to DGUs must guarantee voltage and frequency stability of the whole ImG. Indeed, design methods for load-connected ImGs could be directly extended to any ImG by performing control design on the reduced network. However, decentralized control schemes for ImGs often rely on additional assumptions, such as specific line models. For instance, droop controllers are tailored to either mainly inductive or mainly resistive lines [11], while Plug-and-Play (PnP) controllers in [1] assume RL lines. This could be a problem as instantaneous KR does not guarantee reduced line models will have the same structure of the original ones, e.g. simple RL lines could result in reduced lines with a more complex dynamics [8]. Even though this does not happen in specific line cases [3, 5], in general, one faces the problem of devising *approximate* instantaneous KR methods for preserving selected features of line models.

In this paper we focus on adapting KR to the PnP design algorithm in [1] devoted to the synthesis of decentralized controllers for AC ImGs. The main advantage of PnP control is that the computation of a local regulator for a DGU does not require a global ImG model but only parameters of lines connected to that DGU. Furthermore, one can test if the addition/removal of a DGU can spoil stability of the whole ImG before performing the operation and by solving a local optimization problem. The method in [1] assumes load-connected ImGs and RL lines. In order to preserve the structure of transfer functions describing lines, we propose an approximate instantaneous KR procedure that we term *hybrid KR (hKR)*, as it combines AC-KR with dynamic line models. We show that hKR reproduces exactly the behavior of voltages and currents at boundary nodes in PSSS, even in the case of unbalanced phases. The design of PnP controllers based on hKR is tested on a 21-bus ImG derived from the IEEE test feeder in [12], enhanced with switches yielding changes of line topology and plug-in/out of DGUs. Simulations performed in PSCAD confirm the applicability of our approach.

The models of DGUs and lines are introduced in Section 2. Section 3 presents the new hKR approach together with simulations showing its features. Results in [1] on PnP control design are briefly reviewed in Section 4. Simulations illustrating the joint use of hKR and PnP design are given in Section 5.

Notation and basic definitions. We use $f^{abc}(t) = [f_a(t), f_b(t), f_c(t)]^T \in \mathbb{R}^3$ for denoting three-phase signals in the *abc* frame. A three-phase signal $f^{abc}(t)$ is balanced if the analytic signals [13] $F_a(t) \exp(i\delta_a(t))$, $F_b(t) \exp(i\delta_b(t))$, $F_c(t) \exp(i\delta_c(t))$ associated to $f_a(t)$, $f_b(t)$, $f_c(t)$, respectively, have the same envelope (i.e. $F_a(t) = F_b(t) = F_c(t)$) and their instantaneous phases are such that $\delta_b(t) = \delta_a(t) - 2\pi/3 = \delta_c(t) + 2\pi/3$ or $\delta_b(t) = \delta_a(t) + 2\pi/3 = \delta_c(t) - 2\pi/3$; in the first

case one has a positive-sequence balanced signal, in the latter a negative-sequence balanced signal [14]. A three-phase signal is unbalanced if it is not balanced. A three-phase network element is balanced if it drains balanced currents when supplied by balanced voltages, with currents of the same sequence (positive or negative) of voltages; otherwise, it is said to be unbalanced [15]. To $f^{abc}(t)$, we associate its representation in the $dq0$ reference frame (i.e. $f^{dq0}(t)$). It is obtained from $f^{abc}(t)$ through the Park transformation [16], denoted with $T(\theta(t))$, $\theta(t) = \omega_0 t$, ω_0 being the nominal network frequency. Since in the present work only signals without zero-sequence component (i.e. $f^0(t) = 0$) are used, we can associate to $f^{abc}(t)$ its complex dq -representation $f^{dq}(t) = f^d(t) + \mathbf{i} f^q(t)$ without loss of generality.

When clear from the context, we omit time dependence of electrical quantities. $\mathcal{L}[\cdot]$ is the Laplace-transform operator. The cardinality of the finite set S will be denoted with $|S|$. According to the definitions in [17], a weighted graph $\mathcal{G} = (\mathcal{V}, \mathcal{E}, W)$ is given by a finite set of nodes $\mathcal{V} = \{1, \dots, n\}$, a set of edges $\mathcal{E} \subseteq \mathcal{V} \times \mathcal{V}$ and a diagonal matrix W of dimension $|\mathcal{E}| \times |\mathcal{E}|$, collecting, on its diagonal, weights W_e , $e \in \mathcal{E}$. In this work, weights can be real numbers, complex numbers or SISO transfer functions (in this case, we replace W with $W(s)$). An edge $e \in \mathcal{E}$ is a self-loop if $e = (i, i)$, for some $i \in \mathcal{V}$. All graphs in this work will not contain self-loops. The order of a graph is $n = |\mathcal{V}|$. A graph is undirected if $(x, y) \in \mathcal{E} \implies (y, x) \in \mathcal{E}$. In this case, the pairs (x, y) and (y, x) are considered as identical and unordered. Otherwise, the graph is said to be directed. The set of neighbors of node $i \in \mathcal{V}$ is $\mathcal{N}_i = \{j : (i, j) \in \mathcal{E} \text{ or } (j, i) \in \mathcal{E}\}$. A graph is said to be connected if there is a path from any vertex to every other vertex of the graph. All graphs considered in this work are connected.

The incidence matrix of \mathcal{G} is denoted with $B \in \mathbb{R}^{|\mathcal{V}| \times |\mathcal{E}|}$ [17]. The Laplacian of \mathcal{G} is the matrix $\mathbb{L} = BWB^T$.

2 Microgrid model

2.1 ImG associated graph

Consider an ImG composed of DGUs and loads, connected through electrical lines. The line network has an arbitrary topology, which we assume to be connected. Without loss of generality, one can represent each ImG as a weighted connected directed graph $\mathcal{G} = (\mathcal{V}, \mathcal{E}, W(s))$ (see Figure 1, for example) where the vertex set \mathcal{V} is partitioned into a set of boundary nodes \mathcal{V}_b and a set of internal nodes \mathcal{V}_ℓ . Subset \mathcal{V}_b identifies Point of Common Coupling (PCC) nodes, i.e. the terminals of each DGU, while \mathcal{V}_ℓ contains load nodes, i.e. loads that are not directly connected to PCCs. Similarly, we denote the nodal currents injected by the DGUs as I_b ; the nodal currents injected by loads are I_ℓ . Nodal currents are positive if entering into nodes. Nodal voltages are partitioned analogously.

Each edge corresponds to an electric line and the orientation of the edges $e_1, \dots, e_{|\mathcal{E}|} \in \mathcal{E}$ is arbitrary. We adopt the following sign convention: reference directions of line currents coincide with edges orientations and voltages V_e , $e = (i, j) \in \mathcal{E}$ are defined as $V_i - V_j$. Finally, the weight of every edge is given by its admittance transfer function $W_e(s)$ accounting for the dynamics of line $e \in \mathcal{E}$.

2.2 DGU and line electrical models

We assume three-phase electrical signals without zero-sequence components and balanced network parameters. Note that we do not assume balanced signals, hence including in our framework the case of unbalanced load currents. As in [18], the electrical scheme of DGU $i \in \mathcal{V}_b$ is represented in Figure 2 and its model in dq coordinates is:

$$\begin{cases} \frac{d}{dt} V_i^{dq} = -\mathbf{i}\omega_0 V_i^{dq} + \frac{I_{ti}^{dq}}{C_{ti}} - \frac{I_{Li}^{dq}}{C_{ti}} - \frac{1}{C_{ti}} I_{bi}^{dq} \\ \frac{d}{dt} I_{ti}^{dq} = -\left(\frac{R_{ti}}{L_{ti}} + \mathbf{i}\omega_0\right) I_{ti}^{dq} - \frac{V_i^{dq}}{L_{ti}} + \frac{V_{ti}^{dq}}{L_{ti}} \end{cases} \quad (1)$$

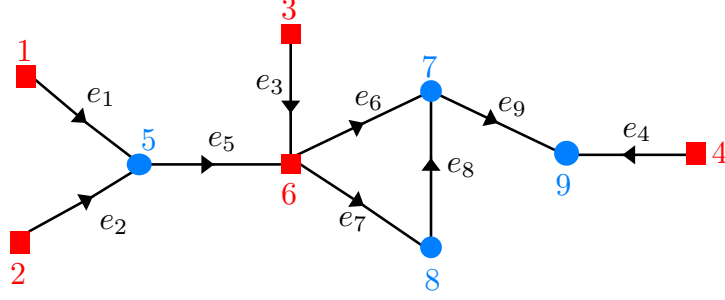


Figure 1: Example of a graph representing the line network of a microgrid. Red squares denote boundary nodes (i.e. DGUs with corresponding local loads I_{Li} , if any), while blue circles represent internal nodes (i.e. loads).

where V_i , I_{ti} , I_{bi} , I_{Li} , V_{ti} , R_{ti} , C_{ti} and L_{ti} are shown in Figure 2.

Remark 1. We highlight that each DGU might present a local load current I_{Li} connected to its PCC and we will treat it as an exogenous disturbance in control design. However, local load currents I_L are different from load currents I_ℓ defined in Section 2.1. The latter ones, in fact, represent the effect of loads that are not directly connected to the terminals of DGUs. ■

In dq reference frame, the three-phase RL line associated to the edge $(i, j) \in \mathcal{E}$ has the dynamics:

$$\frac{d}{dt} I_{ij}^{dq} = - \left(\frac{R_{ij}}{L_{ij}} + i\omega_0 \right) I_{ij}^{dq} + \frac{1}{L_{ij}} (V_i^{dq} - V_j^{dq})$$

where I_{ij} is shown in Figure 2. Equivalently, in term of transfer functions, one has $I_{ij}^{dq}(s) = W_{ij}(s) (V_i^{dq}(s) - V_j^{dq}(s))$ with:

$$W_{ij}(s) = \frac{1}{Z_{ij} + L_{ij}s}, \quad Z_{ij} = R_{ij} + i\omega_0 L_{ij}. \quad (2)$$

Consider an ImG composed of n nodes partitioned into n_b boundary nodes and $n_\ell = n - n_b$ internal nodes. If $n = n_b$ and $n_\ell = 0$, then we term the microgrid “load-connected” as the current loads appear only at PCC of DGUs. Otherwise, let us set: $I^{dq} = [I_b^{dq^T}, I_\ell^{dq^T}]^T$, where $I_b^{dq} = [I_{b_1}^{dq}, \dots, I_{b_{n_b}}^{dq}]^T$ and $I_\ell^{dq} = [I_{\ell_1}^{dq}, \dots, I_{\ell_{n_\ell}}^{dq}]^T$. If $b_k = i$, the boundary current $I_{b_k}^{dq}$ is the current I_{bi}^{dq} injected by DGU i . Nodal voltages $V^{dq} = [V_b^{dq^T}, V_\ell^{dq^T}]^T$ are partitioned analogously. In order to account for the network interconnections, by applying KCL and KVL laws one obtains [8]:

$$\begin{pmatrix} I_b^{dq}(s) \\ I_\ell^{dq}(s) \end{pmatrix} = \begin{pmatrix} \mathbb{L}_{bb}(s) & \mathbb{L}_{b\ell}(s) \\ \mathbb{L}_{\ell b}(s) & \mathbb{L}_{\ell\ell}(s) \end{pmatrix} \begin{pmatrix} V_b^{dq}(s) \\ V_\ell^{dq}(s) \end{pmatrix} \quad (3)$$

that is $I^{dq}(s) = \mathbb{L}(s)V^{dq}(s)$ where $\mathbb{L}(s)$ is the graph Laplacian of the graph \mathcal{G} with weights $W_{ij}(s)$. By construction, one has $\mathbb{L}_{ij}(s) = -W_{ij}(s)$ if $(i, j) \in \mathcal{E}$ and $\mathbb{L}_{ii}(s) = -\sum_{j \in \mathcal{N}_i} \mathbb{L}_{ij}(s)$.

3 Methods for KR

KR [2] is a reduction method for eliminating internal nodes in an electrical network while preserving relevant features of voltages and currents at boundary nodes. In our setup, internal nodes correspond to load nodes.

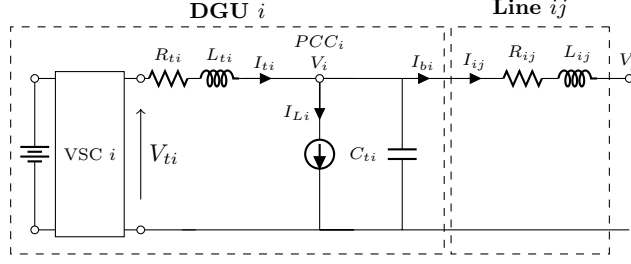


Figure 2: Equivalent single-phase electrical scheme of DGU i composed of a Voltage Source Converter (VSC), an RLC filter, a local load I_{Li} and a single RL line connecting DGU i with the node $j \in \mathcal{V}$.

We first summarize two existing approaches (*instantaneous* KR and AC-KR). Then, we present hKR in Section 3.1 and illustrate its performance through simulations in Section 3.2.

Assuming $\mathbb{L}_{\ell\ell}(s)$ in (3) is invertible¹ for some $s \in \mathbb{C}$, we have [8]:

$$I_b^{dq}(s) = \mathcal{K}(\mathbb{L}(s)) V_b^{dq}(s) - \mathcal{T}(s) I_\ell^{dq}(s) \quad (4a)$$

$$\mathcal{K}(\mathbb{L}(s)) = \mathbb{L}_{bb}(s) - \mathbb{L}_{b\ell}(s) \mathbb{L}_{\ell\ell}^{-1}(s) \mathbb{L}_{\ell b}(s) \quad (4b)$$

$$\mathcal{T}(s) = -\mathbb{L}_{b\ell}(s) \mathbb{L}_{\ell\ell}^{-1}(s). \quad (4c)$$

We term $\mathcal{K}(\cdot)$ the *KR operator* and $\mathcal{T}(s)$ the *accompanying matrix* of $\mathbb{L}(s)$. From (4a), $\mathcal{T}(s)$ provides an equivalent vector of currents

$$\tilde{I}_b^{dq}(s) = \mathcal{T}(s) I_\ell^{dq}(s) \quad (5)$$

to be injected in the boundary nodes.

The matrix $\mathbb{L}_{red}(s) = \mathcal{K}(\mathbb{L}(s))$ is still the Laplacian of a directed graph $\mathcal{G}_{red} = (\mathcal{V}_b, \mathcal{E}_{red}, W_{red}(s))$ [8] that is uniquely defined (up to the orientation of edges, which can be arbitrarily chosen) and that has weights $W_{red,ij}(s) = -(\mathbb{L}_{red}(s))_{ij}$ for $(i, j) \in \mathcal{E}_{red}$. \mathcal{G}_{red} is called the *Kron reduced* graph.

Note that, for given loads $I_\ell^{dq}(t)$ and voltages $V_b^{dq}(t)$, $t \geq 0$, if initial states of DGUs and lines are zero, then currents $I_b^{dq}(t)$ computed through (3) and (4a) are identical at all times. For this reason, (4a), along with the graph \mathcal{G}_{red} , can be termed *instantaneous* KR [5, 8].

Remark 2. A key issue is to understand when weights $W_{red,ij}(s)$ can be written as in (2) replacing R_{ij} and L_{ij} with suitable parameters \tilde{R}_{ij} and \tilde{L}_{ij} . It has been shown that this is guaranteed only under special assumptions, for instance if original lines are homogeneous, i.e. $\frac{R_{e1}}{L_{e1}} = \frac{R_{e2}}{L_{e2}}$, $\forall e_1, e_2 \in \mathcal{E}$ [5]. In this case, one also has $\tilde{R}_{ij} > 0$ and $\tilde{L}_{ij} > 0$. ■

Next, we introduce AC-KR. Since the three-phase RL line network is balanced and no zero-sequence signals are present, it can be split into three independent and identical single-phase circuits. Each one is associated with the “single-phase” directed graph $\mathcal{G}^{sp} = (\mathcal{V}, \mathcal{E}, W^{sp}(s))$ where transfer functions $W_{ij}^{sp}(s) = 1/(R_{ij} + sL_{ij})$ represent, independently of the phase $\star = \{a, b, c\}$, the relation between $\mathcal{L}[V_i^\star(t) - V_j^\star(t)]$ and $\mathcal{L}[I_{ij}^\star(t)]$. When the network is in PSSS with frequency ω_0 , then $V_i^\star(t) = A_i^\star \sin(\omega_0 t + \phi_i^\star)$ and $I_i^\star(t) = B_i^\star \sin(\omega_0 t + \gamma_i^\star)$, $\forall i \in \mathcal{V}$. Moreover, we can associate each sinusoid $V_i^\star(t)$ to the corresponding phasor $\tilde{V}_i^\star = A_i^\star \exp(i\phi_i^\star)$. Current phasors \tilde{I}_i^\star are defined analogously. Let us define vectors $\tilde{\mathbf{V}}^\star = [\tilde{V}_1^\star, \tilde{V}_2^\star, \dots, \tilde{V}_n^\star]^T$ and $\tilde{\mathbf{I}}^\star = [\tilde{I}_1^\star, \tilde{I}_2^\star, \dots, \tilde{I}_n^\star]^T$, $\star \in \{a, b, c\}$. In PSSS with frequency ω_0 , the relation between nodal currents and nodal voltages, for each phase, is given by: $\tilde{\mathbf{I}}^\star = \mathbb{L}^{AC} \cdot \tilde{\mathbf{V}}^\star$, $\star \in \{a, b, c\}$, where $\mathbb{L}_{ij}^{AC} = -1/Z_{ij}$, if $(i, j) \in \mathcal{E}$, and $\mathbb{L}_{ii}^{AC} = \sum_{j \in \mathcal{N}_i} 1/Z_{ij}$. In particular, $\mathbb{L}^{AC} = \mathbb{L}(0)$ by construction.

¹Conditions for the invertibility of $\mathbb{L}_{\ell\ell}(s)$ have been studied in [8].

Definition 1. Let \vec{V}^* , \vec{I}^* and \mathbb{L}^{AC} be partitioned into boundary and internal components as in (3) and assume $\mathbb{L}_{\ell\ell}^{AC}$ is invertible². AC-KR is given by the graph $\mathcal{G}_{red}^{AC} = (\mathcal{V}_b, \mathcal{E}_{red}, W_{red}^{AC})$ associated to $\mathcal{K}(\mathbb{L}^{AC})$ (up to the orientation of edges, which can be arbitrarily chosen) and

$$\vec{I}_b^* = \mathcal{K}(\mathbb{L}^{AC}) \vec{V}_b^* - \mathcal{T}^{AC} \vec{I}_\ell^* \quad (6)$$

$$\mathcal{T}^{AC} = -\mathbb{L}_{b\ell}^{AC} (\mathbb{L}_{\ell\ell}^{AC})^{-1}. \quad (7)$$

We highlight that (7) corresponds to (4c) when $\mathbb{L}(s)$ is replaced by \mathbb{L}^{AC} . Furthermore, (6) provides a relation analogous to (4a).

3.1 Hybrid KR

We extend the application of AC-KR to three-phase electrical variables not necessarily in PSSS.

Definition 2. The approximate Kron reduced graph \mathcal{G}_{red}^A of the original network \mathcal{G} is obtained by:

- 1) computing $\mathbb{L}_{red}^{AC} = \mathcal{K}(\mathbb{L}^{AC})$ and the associated directed graph $\mathcal{G}_{red}^{AC} = (\mathcal{V}_b, \mathcal{E}_{red}, W_{red}^{AC})$;
- 2) setting $\mathcal{G}_{red}^A = (\mathcal{V}_b, \mathcal{E}_{red}, W_{red}^A(s))$ where, for $(i, j) \in \mathcal{E}_{red}$

$$W_{red,ij}^A(s) = \frac{1}{\tilde{Z}_{ij} + \tilde{L}_{ij}s}, \quad (8)$$

$$\tilde{Z}_{ij} = -(\mathbb{L}_{red}^{AC})_{ij}^{-1}, \tilde{L}_{ij} = \frac{1}{\omega_0} \text{Im}(\tilde{Z}_{ij}) \quad (9)$$

In other words, in \mathcal{G}_{red}^A , line impedances have still the dynamics (2) but resistances $\tilde{R}_{ij} = \tilde{Z}_{ij} - i\omega_0 \tilde{L}_{ij}$ and inductances \tilde{L}_{ij} are those predicted by AC-KR. Note also that, by construction, graphs associated to \mathbb{L}_{red}^{AC} and $\mathbb{L}_{red}(s)$ have the same set of undirected edges. Therefore, choosing the same orientation, the set of directed edges of \mathcal{G}_{red} and \mathcal{G}_{red}^{AC} can be made identical (this is why they have been both denoted with \mathcal{E}_{red}).

Remark 3. AC-KR does not guarantee positivity of the reduced resistances and inductances [8]. Based on the results of [5], one expects that negative values can occur if the time constants of the original lines are spread in a wide range. In microgrids, however, electrical lines are usually similar and so are their time constants. ■

In order to complete the KR procedure and specify a formula analogous to (4a), it remains to be seen how to compute equivalent boundary currents due to the effects of internal currents that have been eliminated.

Definition 3. hKR is given by the network \mathcal{G}_{red}^A and the relation

$$I_b^{dq}(s) = \mathbb{L}_{red}^A(s) V_b^{dq}(s) - \tilde{I}_b^{dq}(s) \quad (10)$$

where $\mathbb{L}_{red}^A(s)$ is the Laplacian of \mathcal{G}_{red}^A and $\tilde{I}_b^{dq}(s)$ is defined in (5).

In other words, in hKR line dynamics is approximated as in (8) but internal currents are mapped into boundary currents with no approximation.

The next result characterizes asymptotic behaviors preserved by hKR.

Proposition 1. Consider the network \mathcal{G} and assume parameters \tilde{R}_{ij} and \tilde{L}_{ij} obtained in hKR are strictly positive. If I_ℓ^{abc} and V_b^{abc} converge to PSSS with angular frequency ω_0 , then the asymptotic behavior of I_b^{dq} computed from (3) is the same as when I_b^{dq} is computed from (10).

²Conditions for the invertibility of $\mathbb{L}_{\ell\ell}^{AC}$ have been studied in [7].

Proof. Due to the equivalence of the electrical quantities of the network in abc and dq reference frames, we use abc coordinates. Since the three-phase RL line network is balanced and no zero-sequence signals are present, we make reference to the single-phase directed graph $\mathcal{G}^{sp} = (\mathcal{V}, \mathcal{E}, W^{sp}(s))$, introduced for illustrating AC-KR. The instantaneous relation between $I^\star(s)$ and $V^\star(s)$, $\star \in \{a, b, c\}$, is given by: $I^\star(s) = \mathbb{L}^{sp}(s)V^\star(s)$, where $\mathbb{L}^{sp}(s)$ is the Laplacian matrix of \mathcal{G}^{sp} . After applying hKR, the Laplace transforms of phase $\star \in \{a, b, c\}$ of signals $I_b^{abc}(t)$, $V_b^{abc}(t)$ and $I_\ell^{abc}(t)$ are related by

$$I_b^\star(s) = \mathbb{L}_{red}^{sp^A}(s)V_b^\star(s) - \mathcal{T}^{sp}(s)I_\ell^\star(s)$$

where $\mathcal{T}^{sp}(s)$ is given by (4c), computed with respect to $\mathbb{L}^{sp}(s)$ and $\mathbb{L}_{red}^{sp^A}$ is the Laplacian of the single-phase approximate Kron reduced graph $\mathcal{G}_{red}^{sp^A} = (\mathcal{V}_b, \mathcal{E}_{red}, W_{red}^{sp^A}(s))$, with weights $W_{red,ij}^{sp^A}(s) = 1/(s\tilde{L}_{ij} + \tilde{R}_{ij})$. We note that, by construction, the poles of all entries of $\mathbb{L}_{red}^{sp^A}$ have strictly negative real parts. Moreover, also the poles of all entries of $\mathcal{T}^{sp}(s)$ have strictly negative real parts. This can be shown as follows. We recall that the RL network associated to \mathcal{G}^{sp} is asymptotically stable because it is strictly passive, and, by construction, (4a) preserves the BIBO stability property between inputs V_b^\star and I_ℓ^\star and output I_b^\star . Hence, in experiments where $V_b^\star = 0$ and only one load current $I_{\ell_i}^\star(t)$ at time is excited, if $I_{\ell_i}^\star(t)$ is bounded, also all elements of $I_b^\star(t)$ are bounded. By the superposition principle, this shows that all elements of $\mathcal{T}^{sp}(s)$ are BIBO stable (and hence asymptotically stable) SISO transfer functions.

Let us consider the case in which all elements of inputs V_b^\star and I_ℓ^\star are sinusoids with angular frequency ω_0 . By the frequency response theorem [19], each element of $I_b^\star(t)$ tends to a sinusoid. Moreover, the relation between the phasors \vec{V}_b^\star , \vec{I}_b^\star and \vec{I}_ℓ^\star is given by: $\vec{I}_b^\star = \mathbb{L}_{red}^{sp^A}(i\omega_0)\vec{V}_b^\star + \mathcal{T}^{sp}(i\omega_0)\vec{I}_\ell^\star$, that is (6).

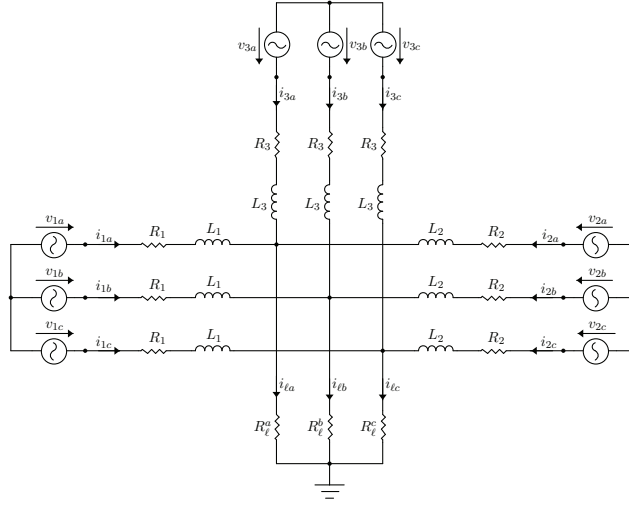
Since the asymptotic quantities in abc coordinates of the original and hybrid Kron reduced network are identical, then they coincide also in dq coordinates. Similar arguments can be also applied to the case when V_b^\star and I_ℓ^\star are not sinusoids, but asymptotically reach PSSS with frequency ω_0 . \square

3.2 Numerical examples

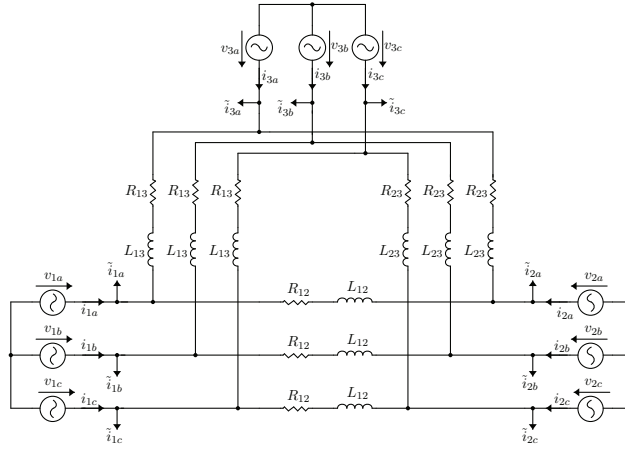
Consider the hKR of the three-phase network in Figure 3a, composed of three ideal voltage sources and balanced RL lines connecting the generators to a purely resistive load. The three-phase voltage generators are balanced and have angular frequency $\omega_0 = 2\pi 50$ rad/s. In this very simple case, hKR is a Y- Δ transformation. The reduced network is shown in Figure 3b. The corresponding voltage generators are identical for the original and reduced networks. Hence, from Proposition 1, we expect I_b in the original and reduced models to be the same, once PSSS is reached. The lines and loads parameters, as well as the voltages of generators, are collected in Tables 2, 3, 4, 5 and 6 in Appendix A.

Example 1 - Linear unbalanced load. In this example, we suppose that the resistive load is unbalanced and compare the original circuit with the hybrid Kron reduced model. Figure 4 shows the output current of phase a of generator 1. This example highlights that hKR ensures asymptotic equivalence, even if the load is unbalanced. In the presented case, the lines are mainly resistive, so equivalence is achieved almost immediately.

Example 2 - Nonlinear load. In this second example, we consider the same network of Example 1, but with the resistive load replaced by a six-pulse bridge rectifier. We compare the currents at boundary nodes of the original circuit with those of the reduced model. For the sake of simplicity, we concentrate on the output currents of generator 1, phase a , shown in Figure 5a. Even if the load currents are highly distorted, the difference between boundary currents of the original and reduced network goes asymptotically to zero, as shown in Figure 5b. This is because Proposition 1 provides a sufficient, but not necessary, condition for asymptotic equivalence of the boundary currents. Analogous results are obtained for all the other phases and generators.



(a) Original network.



(b) Reduced model obtained from hKR.

Figure 3: Original and reduced networks.

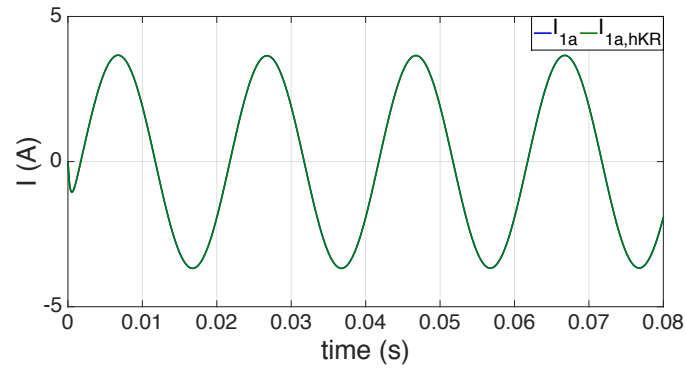


Figure 4: Example 1 - Comparison between original (blue line) and reduced (green line) phase a currents of generator 1 with unbalanced load.

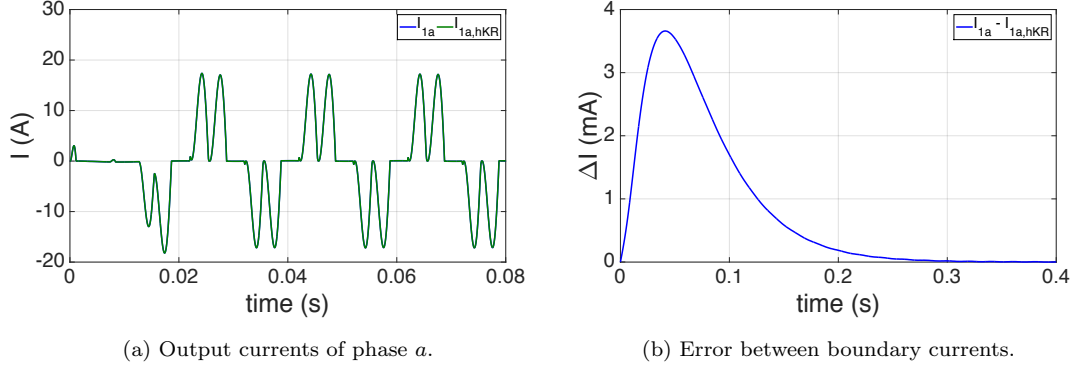


Figure 5: Example 2 - Comparison between original and reduced currents of phase a of generator 1 with nonlinear load.

4 PnP control of ImGs

In this Section we briefly summarize the PnP algorithm in [1] for designing a decentralized control architecture guaranteeing voltage and frequency stability in an ImG. Then, we will show how to generalize it to the case of ImGs with arbitrary topologies. The method in [1] assumes a load-connected topology and RL lines with strictly positive resistances and inductances. Local regulators \mathcal{C}_i use measurements of the voltage V_i^{dq} at PCC (see Figure 2) and the current I_{ti}^{dq} to control the voltage V_{ti}^{dq} at the VSC i so as to make V_i^{dq} track a reference signal. Furthermore, each controller is composed of a matrix gain and an integral action on the d and q components of the tracking error. When a DGU (say DGU i) wants to join the network (e.g. DGU 3 in Figure 6), it issues a plug-in request to its future neighbors, i.e. DGUs $j \in \mathcal{N}_i$ (see, for example, DGUs 2 and 4 in Figure 6). DGU i then solves the Linear Matrix Inequality (LMI) problem (19) in [1], which depends only upon the parameters of the lines ij . If feasible, the optimization problem produces a controller \mathcal{C}_i , along with a local and structured Lyapunov function that can be used for certifying stability of the whole ImG. Since also DGUs $j \in \mathcal{N}_i$ will have a new neighbor, they must update their controller \mathcal{C}_j by taking into account the parameters of the new line ji . This is done by solving an LMI problem analogous to the one solved by DGU i . If one of the above LMI problems is unfeasible, plug-in of DGU i is denied. Otherwise, DGU i can be connected and stability of the whole ImG can be certified using the sum of the computed local Lyapunov functions.

Unplugging of a DGU (say DGU m) follows a similar procedure: as line mk , $k \in \mathcal{N}_m$ will be disconnected from the corresponding DGU k , all controllers \mathcal{C}_k must be successfully redesigned before allowing the disconnection. Following a similar reasoning, also the possibility of changing a parameter of line ij (or add a new line ij), must be first tested by successfully designing controllers \mathcal{C}_i and \mathcal{C}_j through suitable LMIs. While line changes are not common in ImGs, they could happen in the hybrid Kron reduced network because of the addition/removal of a load node in the original ImG. Examples of this phenomenon are provided in the next Section. We also highlight that PnP controllers in [1] can be enhanced with pre-filters of reference signals and compensators of (measured) load currents I_{Li} represented in Figure 2.³

When the design of PnP controllers is conducted with reference to the hybrid Kron reduced model, according to the electrical scheme in Figure 2, current $\tilde{I}_{b_k}^{dq}$ in (10) can be lumped into current I_{Li}^{dq} , if $b_k = i$. In other words, the effect of load nodes is mapped into additional contributions to DGU loads. This is, however, not critical because DGU loads are treated as disturbances by PnP controllers.

³These enhancements are optional and they will be not used in the simulations in Section 5.

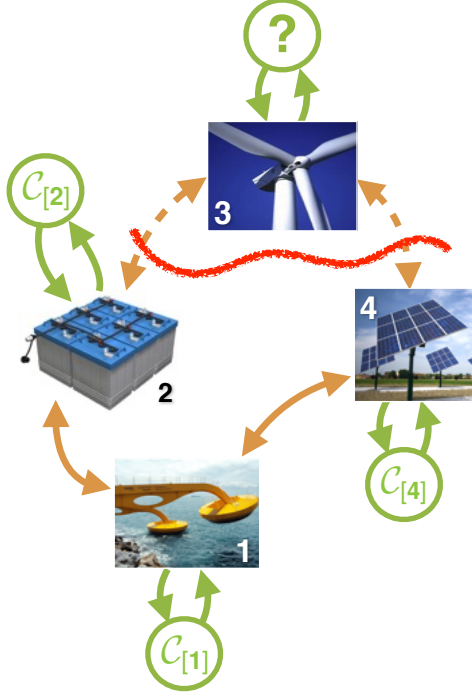


Figure 6: Example of plug-in request issued by DGU 3 to its future neighbors (i.e. DGUs 2 and 4).

4.1 PnP design for general ImGs

Let us consider an ImG with arbitrary topology represented by the directed connected graph \mathcal{G} with node set \mathcal{V} . When a DGU or a load node (say node i) wants to plug in, the first step consists in updating \mathcal{G} accordingly, so obtaining the graph \mathcal{G}^{new} . Then, hKR is applied to \mathcal{G}^{new} for obtaining the reduced ImG $\mathcal{G}_{red}^{A,new}$ with load-connected topology. If some resistances or inductances of reduced lines are negative, the plugging-in of node i is denied, as one of the assumption of the PnP algorithm in [1] is not fulfilled. Otherwise, one compares the reduced graphs \mathcal{G}_{red}^A (associated to \mathcal{G}) and $\mathcal{G}_{red}^{A,new}$ for finding the set $\mathcal{U} \subseteq \mathcal{V}_b$ of DGUs that have new neighbors or that are connected to lines whose impedance has changed. The LMI problem (19) in [1] is then solved for all DGUs $j \in \mathcal{U}$ (and also for $j = i$, if node i is a DGU), hence producing new controllers \mathcal{C}_j . If no LMI is infeasible, controllers in the original ImG are updated and connection of node i is allowed.

Unplugging of a node can be performed in a similar way.

Remark 4. According to the above algorithm, hKR is performed in a centralized fashion every time there is a change in the network topology. This is in contrast with PnP design, whose main feature is to avoid any centralized computations. In the future, we will study how to perform hKR in a distributed fashion. Notably, one can develop this generalization according to the iterative KR procedure [4] proposed for both AC networks in PSSS and resistive networks. In a similar spirit, we will study how to avoid the centralized computation of the set \mathcal{U} by exploiting existing distributed algorithms for path-finding over directed graphs. ■

5 Simulation of a 21-bus network

In this Section, we assess the capability of PnP control and hKR to deal with networks characterized by complex topologies. In particular, we use a network derived from the top half of IEEE 37 topology [12] and identify generation nodes and loads as in [20].

The simulation, whose duration is 13 seconds, has been performed in PSCAD.

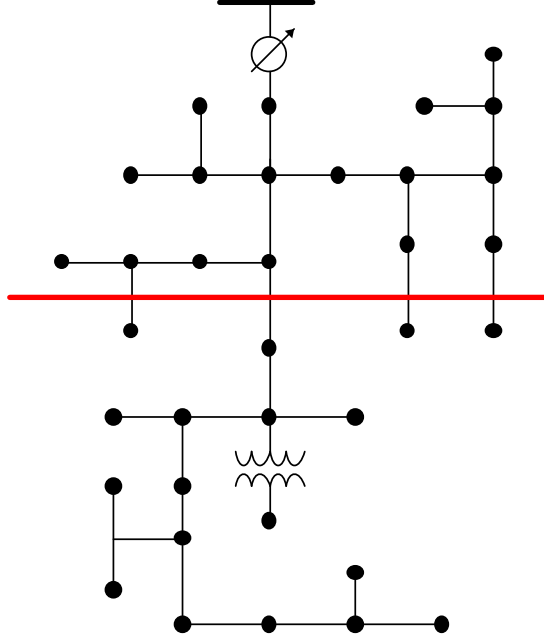


Figure 7: IEEE 37 Node Test Feeder and the top half network considered in our experiments.

5.1 ImG topology

The lack in literature of standard test benches for microgrids has led many authors to use IEEE test feeders [12] as workbenches for microgrids testing. These networks have been originally developed as standards for power flows studies in high-voltage radial grids. When the IEEE test feeders are applied to microgrids, only the network topologies are preserved, while line parameters and loads are changed. In literature, IEEE 37 network, with 37 nodes, appears to be a widespread topology [21], [20]. The IEEE 37 network, shown in Figure 7, has a radial topology, which is quite common in its original context of high/medium-voltage networks. However, microgrids could present more complex topologies (for example, they may have a meshed structure). As a consequence, IEEE 37 appears very simple for PnP control purposes, because it does not contain any loop. In order to show the versatility of the approach based on PnP control and hKR, we have proposed a new network, derived from the top half of IEEE 37 topology in Figure 7.

The proposed topology is shown in Figure 8. It has 21 nodes, with six DGUs, electrical RL lines having time constants spread in a wide range, linear R and RL loads, as well as highly nonlinear and highly inductive loads. Notice that all these loads appear as internal nodes and, without loss of generality, no load I_{Li} directly connected to each PCC is present. Compared to the IEEE 37 network, a switch SW_1 has been introduced, allowing the plugging-in/unplugging of loads at nodes 16, 17 and 18. Moreover, two branches (e_{18} and e_{19}) were added and connected to the microgrid through switches SW_2 e SW_3 respectively. The edge e_{18} creates a mesh between DGUs 1, 3 and 4; this enables us to show that PnP controllers can stabilize also meshed networks. The edge e_{19} simply changes the impedance between DGUs 3 and 5 (as long as SW_1 is closed). Finally, one generation node (21) and two loads (at nodes 19 and 20) have been introduced, so as to simulate the plugging-in of a new DGU. The new generation unit is connected to the microgrid via switch SW_4 .

The lines parameters of the original network are collected in Table 7, in Appendix B. These parameters have been chosen so that the time constants are spread in a wide range; this fact let us show that PnP control can stabilize networks made of lines with very different characteristics.

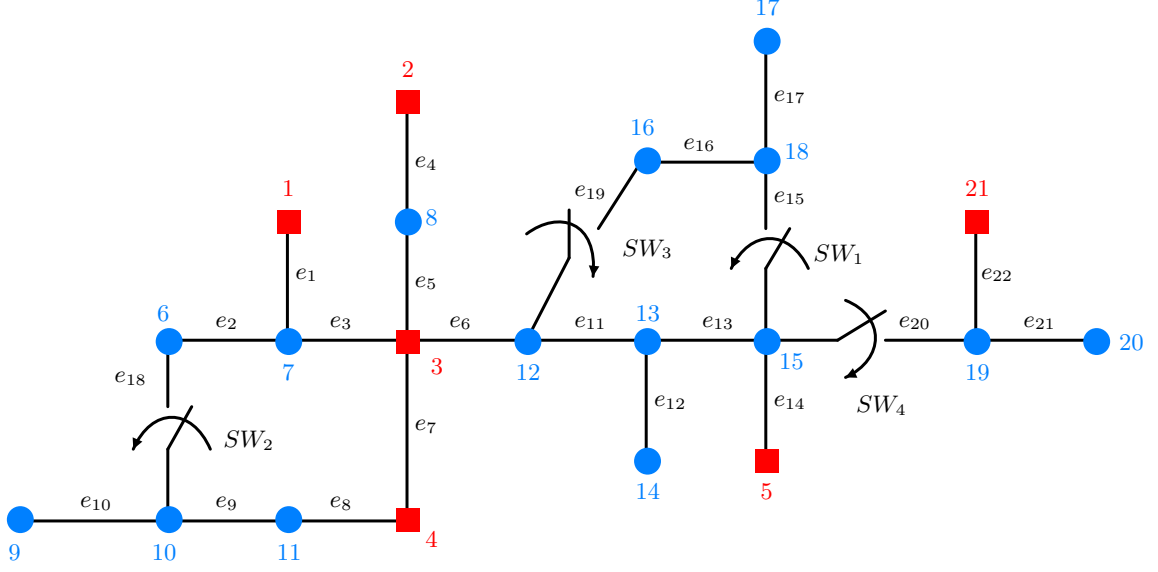


Figure 8: The proposed 21-bus network. Red squares denote boundary nodes (DGUs), blue circles represent interior nodes (loads).

As regards the loads connected to the buses, they are listed in Tables 8 and 9 in Appendix B.

At time $t = 0$ s, there is no energy stored in all inductors and capacitors and all the switches are open. At instant $t = 5$ s, switch SW_1 closes: the overall effect is an increase in electrical loads, mainly supplied by DGUs 3 and 5. Then, SW_2 e SW_3 close respectively at instants $t = 6.5$ s and $t = 8$ s, connecting new branches to the network. Finally, at $t = 9.5$ s switch SW_4 closes, so that the sixth generation unit is connected to the microgrid. Table 1 summarizes the commutations sequence.

Time [s]	Event	SW_1	SW_2	SW_3	SW_4
0	Start simulation	open	open	open	open
5	SW_1 closes	closed	open	open	open
6.5	SW_2 closes	closed	closed	open	open
8	SW_3 closes	closed	closed	closed	open
9.5	SW_4 closes	closed	closed	closed	closed
13	End simulation	closed	closed	closed	closed

Table 1: Simulation time events.

5.2 PnP control design

As described in Section 4.1, the first step in control design consists in applying hKR for obtaining an equivalent ImG with a load-connected topology. Equivalent line impedances are obtained as in (9) with $\omega_0 = 2\pi 50$ rad/s. The reduced network actually depends on the state of the switches in the original network. As long as SW_2 , SW_3 and SW_4 are open, the network in Figure 8 has a radial topology. In particular, the equivalent impedance between nodes 3 and 5 is equal to the sum of the impedances of edges e_6 , e_{11} , e_{13} and e_{14} , irrespectively of the state of switch SW_1 . On the

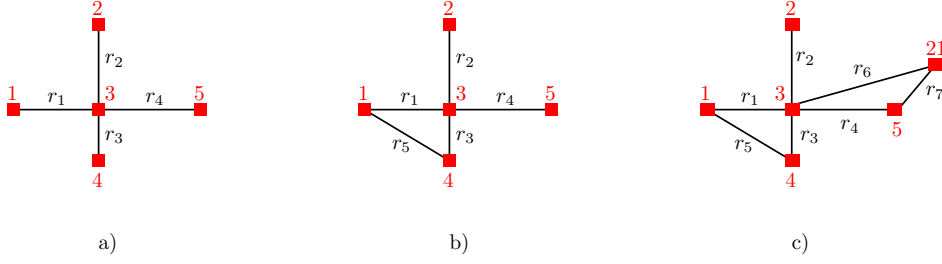
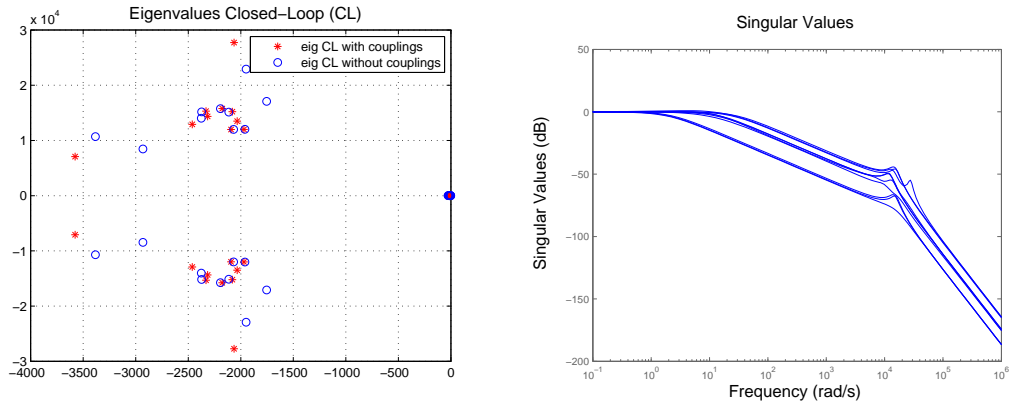


Figure 9: Hybrid Kron reduced networks. Figures a)-b) and c) show the equivalent network for $t \leq 6.5$ s, $6.5 \leq t \leq 9.5$ s and $t \geq 9.5$ s, respectively.

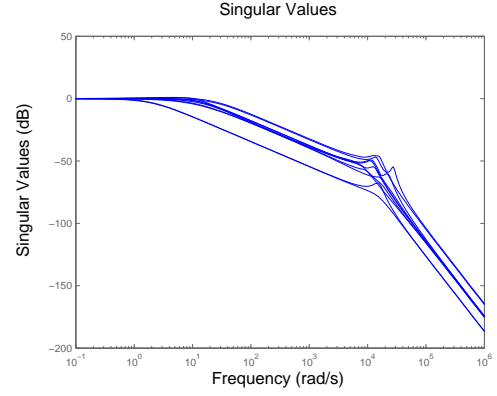
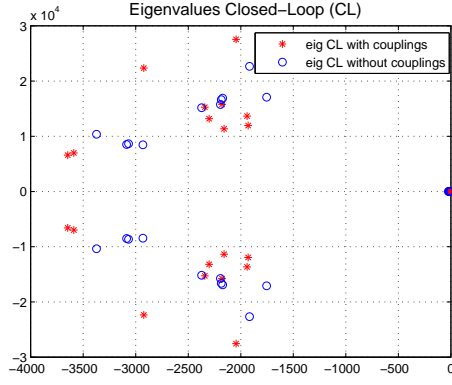
contrary, when switches SW_2 , SW_3 and SW_4 are closed, the topology of the hybrid Kron reduced network and its impedances change. Figure 9 collects the reduced networks that arise during the simulation. In particular, Figure 9a holds when all the four switches are open, or when only SW_1 is closed. The network in Figure 9b refers to the case when SW_2 and SW_3 become closed. The diagram in Figure 9c, instead, holds when all the four switches are closed. The resistances and inductances of the Kron reduced circuits are listed in Tables 10, 11, 12 and 13 in Appendix B. Notably, we remark that, for the three reduced networks, all the equivalent resistances and inductances are positive. At instant $t = 5$ s, SW_1 closes, but the hybrid Kron reduced network does not change, and no redesign of the controllers is needed. Indeed, the only effect of load currents in 16, 17, 18 is to change the term $\tilde{I}_b(s)$ in (10), which is lumped, anyway, in the disturbance loads attached to the PCCs of DGUs. At instant $t = 6.5$ s, the equivalent impedances between nodes 1, 3 and 4 change: the controllers of DGUs 1, 3 and 4 must be redesigned (all the other controllers do not change). At instant $t = 8$ s, the equivalent impedance between boundary nodes 3 and 5 changes: the corresponding DGUs must update their controllers. At $t = 9.5$ s, DGU 21 is connected to the microgrid: controllers of DGUs 3 e 5 must be redesigned again.

The proposed controllers effectively stabilize the microgrid: this is illustrated by Figures 10 -13. These figures show, for every configuration of the switches, the singular values of the closed loop QSL microgrid, as well as its eigenvalues, with and without couplings. In particular, Figures 10a, 11a, 12a and 13a show that all the eigenvalues are on the left half-plane.



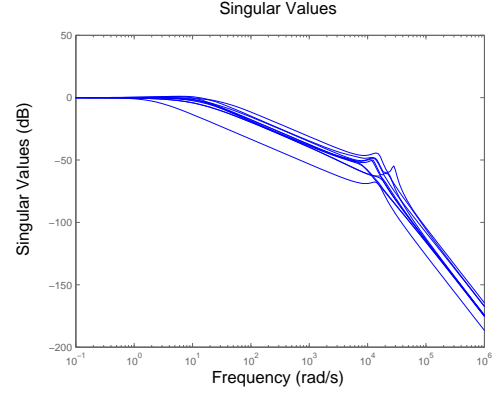
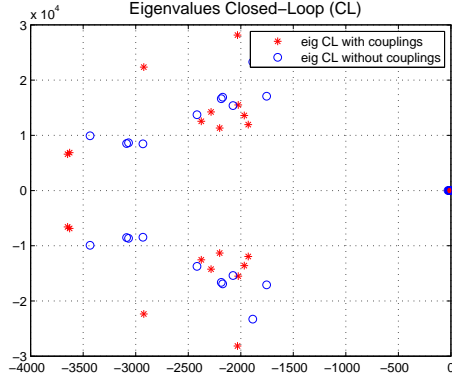
(a) Eigenvalues of the closed-loop (CL) QSL microgrid (b) Singular values of the closed-loop (CL) QSL microgrid. with (red) and without (blue) couplings.

Figure 10: Eigenvalues and singular values of the QSL microgrid when all the switches are open, or only SW_1 is closed.



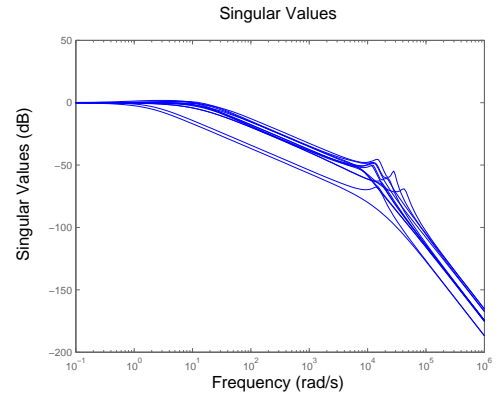
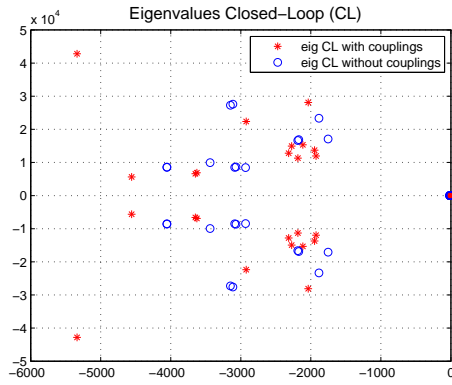
(a) Eigenvalues of the closed-loop (CL) QSL microgrid with (red) and without (blue) couplings. (b) Singular values of the closed-loop (CL) QSL microgrid.

Figure 11: Eigenvalues and singular values with SW_1 , SW_2 closed, and SW_3 , SW_4 open.



(a) Eigenvalues of the closed-loop (CL) QSL microgrid with (red) and without (blue) couplings. (b) Singular values of the closed-loop (CL) QSL microgrid.

Figure 12: Eigenvalues and singular values when SW_1 , SW_2 , SW_3 are closed, and SW_4 open.



(a) Eigenvalues of the closed-loop (CL) QSL microgrid with (red) and without (blue) couplings. (b) Singular values of the closed-loop (CL) QSL microgrid.

Figure 13: Eigenvalues and singular values of the QSL microgrid when all the switches are closed.

5.3 Simulation results

The reference signals for all the generation units are $V_d^{\text{ref}} = \sqrt{2} \cdot 230 \text{ V}$ and $V_q^{\text{ref}} = 0 \text{ V}$. Figure 14 shows the Root Mean Square (RMS) voltage, frequency and Total Harmonic Distortion⁴ (THD) of phase a at the PCCs of the boundary nodes (i.e nodes 1, 2, 3, 4, 5 and 21), respectively. We highlight that, in spite of all the variations of the ImG topology, PnP decentralized control ensures good tracking of voltage references for all DGUs (see Figure 14a). We note that real-time switch between different controllers has been implemented using a bumpless control transfer scheme similar to the one used in classical PID regulators [23]. This guarantees control variables do not have sudden variations at switching times. In our case, bumpless controllers are effective in limiting voltage surges and dips to a few volts when updates of controllers take place (for $t \geq 4 \text{ s}$, the maximal deviation from the reference RMS voltage is of less than 20 volts). Figure 14b shows that the impact of the topology commutations is minor also on the frequency profiles. In fact, PnP controllers promptly restore the frequencies to the nominal value, ensuring negligible variations (i.e. less than 0.5 Hz when the highly inductive load is connected and less than 0.1 Hz when other events occur). Furthermore, from Figure 14c, we notice that THD values are below the maximum limit (5%) recommended in [22].

To evaluate the voltage imbalance at boundary nodes, we calculate the ratio V_N/V_P (expressed in %), where V_N and V_P are the magnitudes of the negative- and positive-sequence components of the phase-to-phase voltage. The time evolution of this ratio is represented in Figure 14d. We notice that it is always below 0.5% which is less than the maximum permissible value (3%) defined by IEEE in [22]. Finally, Figures 14e and 14f show respectively the active and reactive power injected into the microgrid by the DGUs. We notice that PnP controllers alone can not guarantee sharing of the reactive power between the connected DGUs (see Figure 14f). This aim can be achieved by means of higher level control schemes. However, the fulfillment of any power flow requirements is outside the scope of this work.

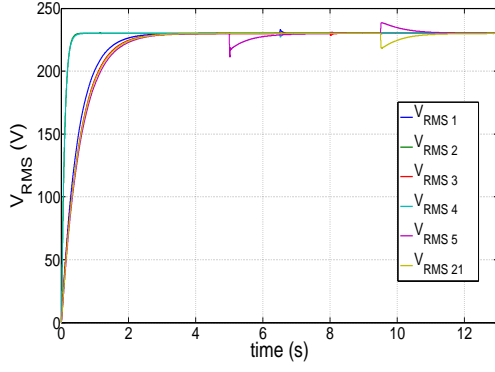
Overall, the fact that voltage and frequency stability is guaranteed even for such a complicated network, proves that hKR is a well suited method for extending the PnP scalable design to ImGs with arbitrary topologies.

6 Conclusions

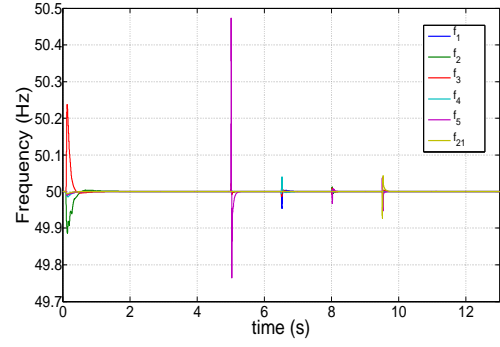
In this paper, we provided a method for extending the PnP control design presented in [1] to AC ImGs with arbitrary topology. We introduced an approximate network reduction algorithm (hKR), based on KR and capable to represent exactly the asymptotic periodic behavior of voltages and currents in the ImG.

As regards the future developments, besides addressing problems described in Remark 4, we aim to extend the hKR also to the case of DC ImGs equipped with PnP controllers [24].

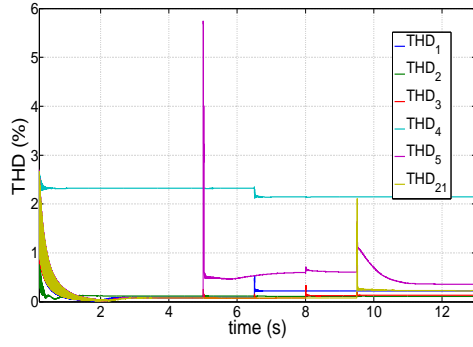
⁴See [22] for a definition.



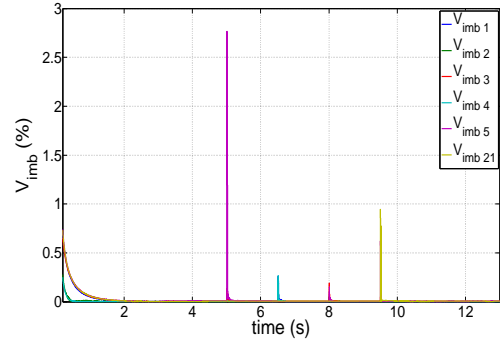
(a) RMS voltages at boundary nodes.



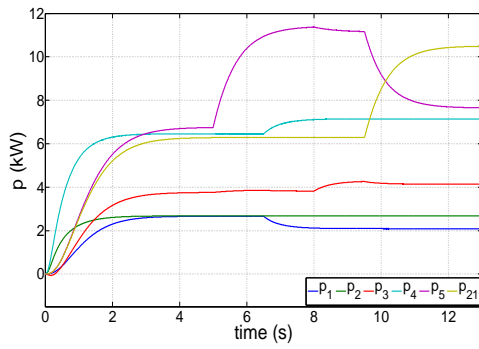
(b) Frequencies at boundary nodes.



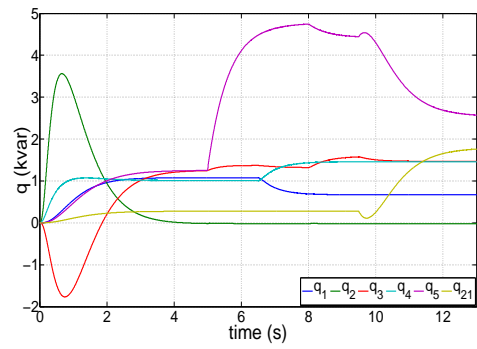
(c) THD at boundary nodes.



(d) Voltage imbalance ratio (V_N/V_P).



(e) Active power at PCC nodes.



(f) Reactive power at PCC nodes.

Figure 14: Performance of PnP control and AC hybrid KR with a 21-bus network.

A Electrical parameters of Examples 1 and 2, Section 3.2

Edge	From node	To node	Resistance [Ω]	Inductance [mH]
e_1	1	4	0.1	2
e_2	2	4	0.2	7
e_3	3	4	1	10

Table 2: Parameters of the original networks of Examples 1 and 2, Section 3.2.

Edge	From node	To node	Resistance [Ω]	Inductance [mH]
e_{12}	1	2	0.2746	10.354
e_{13}	1	3	1.4482	14.8132
e_{23}	2	3	3.9315	52.3706

Table 3: Parameters of the reduced networks of Examples 1 and 2, Section 3.2.

Phase	Resistance [Ω]
a	100
b	10
c	0.01

Table 4: Load parameters of Example 1, Section 3.2.

Name	Description	Values
C_f	Filter capacitance of the rectifier	235 μF
L_f	Filter inductance of the rectifier	84 μH
R_L	Load resistance	40 Ω

Table 5: Parameters of the six-pulse bridge rectifier of Example 2, Section 3.2.

Voltage source	Voltage [V]
v_{1a}	$\sqrt{\frac{2}{3}}399.8 \sin(\omega_0 t)$
v_{2a}	$\sqrt{\frac{2}{3}}400 \sin(\omega_0 t)$
v_{3a}	$\sqrt{\frac{2}{3}}400.2 \sin(\omega_0 t)$
v_{1b}	$\sqrt{\frac{2}{3}}399.8 \sin(\omega_0 t - \frac{2\pi}{3})$
v_{2b}	$\sqrt{\frac{2}{3}}400 \sin(\omega_0 t - \frac{2\pi}{3})$
v_{3b}	$\sqrt{\frac{2}{3}}400.2 \sin(\omega_0 t - \frac{2\pi}{3})$
v_{1c}	$\sqrt{\frac{2}{3}}399.8 \sin(\omega_0 t + \frac{2\pi}{3})$
v_{2c}	$\sqrt{\frac{2}{3}}400 \sin(\omega_0 t + \frac{2\pi}{3})$
v_{3c}	$\sqrt{\frac{2}{3}}400.2 \sin(\omega_0 t + \frac{2\pi}{3})$

Table 6: Voltage values of generators in Examples 1 and 2, Section 3.2.

B 21-bus network

This appendix lists the electrical parameters of the 21-bus network shown in Section 5. The resistances and inductances of the RL lines of network in Figure 8 are collected in Table 7. The

Edge	From node	To node	Resistance [Ω]	Inductance [mH]
e_1	1	7	1	20
e_2	6	7	0.1	1.8
e_3	3	7	1	200
e_4	2	8	0.6	6
e_5	8	3	0.4	35
e_6	3	12	0.1	1.8
e_7	3	4	1	600
e_8	4	11	0.1	2
e_9	10	11	0.1	2.5
e_{10}	9	10	0.2	4.5
e_{11}	12	13	1.1	300
e_{12}	13	15	1	40
e_{13}	13	14	0.1	2
e_{14}	14	5	0.3	8
e_{15}	14	18	0.1	1
e_{16}	16	18	0.3	30
e_{17}	17	18	0.1	2
e_{18}	6	10	1.1	20
e_{19}	12	16	2.1	300
e_{20}	14	19	0.5	10
e_{21}	19	20	0.3	7
e_{22}	19	21	0.1	1.8

Table 7: Parameters of the original 21-bus network.

loads connected to the buses are listed in Tables 8 and 9.

As regards the parameters of the hybrid Kron reduced networks shown in Figure 9, we highlight that they are all positive (i.e. the nature of the original circuits is preserved). In particular, the reduced parameters, when all the four switches are open, are listed in Table 10. Table 11 shows the reduced R and L when SW_1 and SW_2 are closed, with SW_3 and SW_4 open. The reduced parameters, relative to the network with SW_1 , SW_2 and SW_3 closed and SW_4 open, are collected in Table 12. Finally, Table 13 is referred to the case with all four switches closed.

Node	Resistance [Ω]	Inductance [H]
6	80	0.2
7	80	0
8	50	0
10	100	0
11	100	0
12	50	0.05
13	100	0
14	50	0
15	60	0
17	3	1
18	45	0.02
19	50	0
20	50	0

Table 8: Linear loads parameters.

Node	Resistance [Ω]	Filter Inductance [μ H]	Filter Capacitance [μ F]
9	80	84	235
16	80	84	235

Table 9: Nonlinear loads connected to the buses.

Edge	From node	To node	Resistance [Ω]	Inductance [mH]
r_1	1	3	2	220
r_2	2	3	1	41
r_3	3	4	1	600
r_4	3	5	1.6	311.8

Table 10: Equivalent parameters when SW_2 , SW_3 and SW_4 are open.

Edge	From node	To node	Resistance [Ω]	Inductance [mH]
r_1	1	3	2.2813	371.9
r_5	1	4	2.6589	48.9
r_2	2	3	1	41
r_3	3	4	1.58	269.7
r_4	3	5	1.6	311.8

Table 11: Equivalent parameters when SW_1 SW_2 are closed, while SW_3 and SW_4 are open.

Edge	From node	To node	Resistance [Ω]	Inductance [mH]
r_1	1	3	2.2813	371.9
r_5	1	4	2.6586	48.9
r_2	2	3	1	41
r_3	3	4	1.58	269.7
r_4	3	5	1.2971	167.7

Table 12: Equivalent parameters when SW_1 , SW_2 and SW_3 are closed, and SW_4 is open.

Edge	From node	To node	Resistance [Ω]	Inductance [mH]
r_1	1	3	2.2813	371.9
r_5	1	4	2.6586	48.9
r_2	2	3	1	41
r_3	3	4	1.58	269.7
r_4	3	5	0.5602	275.4
r_6	3	21	6.1756	408.1
r_7	5	21	0.9486	20.4

Table 13: Equivalent parameters when all the four switches are open.

References

- [1] S. Rivero, F. Sarzo, and G. Ferrari-Trecate, “Plug-and-play voltage and frequency control of islanded microgrids with meshed topology,” *IEEE Transactions on Smart Grid*, vol. 6, no. 3, pp. 1176–1184, 2015.
- [2] G. Kron, *Tensor analysis of networks*. John Wiley and Sons, 1939.
- [3] A. Van der Schaft, “Characterization and partial synthesis of the behavior of resistive circuits at their terminals,” *Systems & Control Letters*, vol. 59, no. 7, pp. 423–428, 2010.
- [4] F. Dörfler and F. Bullo, “Kron reduction of graphs with applications to electrical networks,” *IEEE Transactions on Circuits and Systems I: Regular Papers*, vol. 60, no. 1, pp. 150–163, 2013.
- [5] S. Y. Caliskan and P. Tabuada, “Kron reduction of power networks with lossy and dynamic transmission lines,” in *Proceedings of the 51st IEEE Annual Conference on Decision and Control (CDC), 2012*. IEEE, 2012, pp. 5554–5559.
- [6] —, “Towards Kron reduction of generalized electrical networks,” *Automatica*, vol. 50, no. 10, pp. 2586–2590, 2014.
- [7] L. Luo and S. V. Dhople, “Spatiotemporal model reduction of inverter-based islanded microgrids,” *IEEE Transactions on Energy Conversion*, vol. 29, no. 4, pp. 823–832, 2014.
- [8] S. V. Dhople, B. B. Johnson, F. Dörfler, and A. O. Hamadeh, “Synchronization of nonlinear circuits in dynamic electrical networks with general topologies,” *IEEE Transactions on Circuits and Systems I: Regular Papers*, vol. 61, no. 9, pp. 2677–2690, 2014.
- [9] J. M. Guerrero, M. Chandorkar, T.-L. Lee, and P. C. Loh, “Advanced control architectures for intelligent microgrids, part I: decentralized and hierarchical control,” *IEEE Transactions on Industrial Electronics*, vol. 60, no. 4, pp. 1254–1262, 2013.
- [10] J. Schiffer, R. Ortega, A. Astolfi, J. Raisch, and T. Sezi, “Conditions for stability of droop-controlled inverter-based microgrids,” *Automatica*, vol. 50, no. 10, pp. 2457–2469, 2014.
- [11] J. M. Guerrero, J. Matas, L. García De Vicuña, M. Castilla, and J. Miret, “Decentralized control for parallel operation of distributed generation inverters using resistive output impedance,” *IEEE Transactions on Industrial Electronics*, vol. 54, no. 2, pp. 994–1004, 2007.
- [12] Distribution Test Feeders, “IEEE PES distribution system analysis subcommittee,” 2011, available: <http://www.ewh.ieee.org/soc/pes/dsacom/testfeeders/index.html>.
- [13] R. Bracewell, *The Fourier Transform and its applications*. New York: McGraw-Hill, 1965.
- [14] G. Cablea, P. Granjon, and C. Berenguer, “Method for computing efficient electrical indicators for offshore wind turbine monitoring,” *Insight-Non-Destructive Testing and Condition Monitoring*, vol. 56, no. 8, pp. 443–448, 2014.
- [15] J. Schiffer, D. Zonetti, R. Ortega, A. Stankovic, T. Sezi, and J. Raisch, “Modeling of microgrids-from fundamental physics to phasors and voltage sources,” *arXiv preprint arXiv:1505.00136*, 2015.
- [16] R. H. Park, “Two-reaction theory of synchronous machines generalized method of analysis-part I,” *Transactions of the American Institute of Electrical Engineers*, vol. 48, no. 3, pp. 716–727, 1929.
- [17] B. Bollobás, *Modern graph theory*, ser. Graduate Texts in Mathematics. Springer Science & Business Media, 1998, vol. 184.

- [18] M. Babazadeh and H. R. Karimi, “A robust two-degree-of-freedom control strategy for an islanded microgrid,” *IEEE Transactions on Power Delivery*, vol. 28, no. 3, pp. 1339–1347, 2013.
- [19] C. A. Desoer and E. S. Kuh, *Basic circuit theory*. Tata McGraw-Hill Education, 1984.
- [20] S. Bolognani and S. Zampieri, “A distributed control strategy for reactive power compensation in smart microgrids,” *IEEE Transactions on Automatic Control*, vol. 58, no. 11, pp. 2818–2833, 2013.
- [21] F. Dörfler, J. Simpson-Porco, and F. Bullo, “Breaking the hierarchy: Distributed control & economic optimality in microgrids,” *arXiv preprint arXiv:1401.1767*, 2014.
- [22] “IEEE recommended practice for monitoring electric power quality,” *IEEE Std 1159-2009 (Revision of IEEE Std 1159-1995)*, pp. c1–81, June 2009.
- [23] K. J. Åström and T. Hägglund, *Advanced PID control*. ISA-The Instrumentation, Systems, and Automation Society; Research Triangle Park, NC 27709, 2006.
- [24] M. Tucci, S. Rivero, J. C. Vasquez, J. M. Guerrero, and G. Ferrari-Trecate, “Voltage control of dc islanded microgrids: a decentralized scalable approach,” in *Proceedings of the 54th IEEE Annual Conference on Decision and Control (CDC), 2015*. IEEE, 2015, to appear.